Original Article

Institution of MECHANICAL ENGINEERS
Journal of POWER AND ENERGY

Proc IMechE Part A:
J Power and Energy
2019, Vol. 233(1) 96–110

DOI: 10.1177/0957650918772658
journals.sagepub.com/home/pia
SAGE

A boil-off gas utilization for improved performance of heavy duty gas turbines in combined cycle

Stefano Mazzoni[1], Srithar Rajoo[2] and Alessandro Romagnoli[3]

Abstract

The storage of the natural gas under liquid phase is widely adopted and one of the intrinsic phenomena occurring in liquefied natural gas is the so-called boil-off gas; this consists of the regasification of the natural gas due to the ambient temperature and loss of adiabacity in the storage tank. As the boil-off occurs, the so-called cold energy is released to the surrounding environment; such a cold energy could potentially be recovered for several end-uses such as cooling power generation, air separation, air conditioning, dry-ice manufacturing and conditioning of inlet air at the compressor of gas turbine engines. This paper deals with the benefit corresponding to the cooling down of the inlet air temperature to the compressor, by means of internal heat transfer recovery from the liquefied natural gas boil-off gas cold energy availability. The lower the compressor inlet temperature, the higher the gas turbine performance (power and efficiency); the exploitation of the liquefied natural gas boil-off gas cold energy also corresponds to a higher amount of air flow rate entering the cycle which plays in favour of the bottoming heat recovery steam generator and the related steam cycle. Benefit of this solution, in terms of yearly work and gain increase have been established by means of ad hoc developed component models representing heat transfer device (air/boil-off gas) and heavy duty 300 MW gas turbine. For a given ambient temperature variability over a year, the results of the analysis have proven that the increase of electricity production and efficiency due to the boil-off gas cold energy recovery has finally yield a revenue increase of 600,000€/year.

Keywords

Boil-off gas, combined cycle, gas turbine, liquefied natural gas, cold energy

Date received: 17 October 2017; accepted: 21 March 2018

Introduction

The continuous increase in energy demand leads to the need to consider additional primary energy sources (PESs) for electricity, cooling, heating and water demand. At the same time, the adoption of various PESs (such as petroleum, natural gas (NG), coal, renewables, biomass, etc.) allows addressing the need for a more sustainable energy production which encompasses environmental, technical and economic viability.[1–3] In line with PESs diversification, NG has been widely investigated as a valid oil replacement. For instance, in the Asian context, in the last few decades, Japan policy has sought to reduce dependence on imported oil by diversifying the energy mix into coal, liquefied natural gas (LNG)[a] and nuclear power.[2] Indeed, the interest in NG as a PES has been continuously increasing over the last decades.[4] The NG utilization between 2025 and 2040 is foreseen to increase by approximately 30 and 60% of the 2014 utilization, respectively, – which is in agreement with International Energy Agency (IEA) predictions.[5] NG availability around the world is approximately 300,000t cubic feet except for the Middle East Peninsula that presents a production 10 times larger.[6] Such a significant NG availability coupled with the worldwide energy demand will lead to more than 460 Mtons of NG crossing the ocean by 2020,[1] mainly stored as LNG. The storage of the NG under

[1]Energy Research Institute @ NTU, Nanyang Technological University, Singapore, Singapore
[2]UTM Centre for Low Carbon Transport in Cooperation with Imperial College, Universiti Teknologi, Skudai, Malaysia
[3]School Mechanical and Aerospace Engineering, Nanyang Technological University, Singapore, Singapore

Corresponding author:
Alessandro Romagnoli, Nanyang Technological University, 50 Nanyang Avenue, Sinagpore 637820, Singapore.
Email: a.romagnoli@ntu.edu.sg

liquid phase is widely adopted and one of the intrinsic phenomena occurring in LNG is the so-called boil-off gas (BoG); this consists of the regasification of the NG due to the ambient temperature and loss of adiabacity in the storage tank.[7] In order to avoid the issues arising from the high-pressure condition due to the BoG, some of the gas should be purged from the storage tank. As the boil-off occurs, the so-called cold energy is released to the surrounding environment; such a cold energy could potentially be recovered for several end-uses like cooling power generation, air separation, air conditioning, dry-ice manufacturing and conditioning of inlet air at the compressor of gas turbine (GT) engines (such as power generation and ships propulsion).[8]

All of the above considerations about the increase in the NG demand go along with the need to reduce the environmental impact of power plants. GT and steam turbine (ST) combined cycles (CC) hold the largest conversion efficiency because of the high peak cycle temperatures and the low heat rejection mean temperature.[9] The possibility of adopting combined cycle gas turbine (CCGT) fed totally or partially by the BoG is an interesting option to improve the system performance and therefore to mitigate pollutants emissions. This paper deals with the possibility of cooling down the inlet air temperature to the GT, by means of internal heat transfer recovery from the LNG BoG cold energy availability. The lower the inlet temperature, the higher the GT performance (power and efficiency); the exploitation of the LNG BoG cold energy also corresponds to a higher amount of air flow rate entering the cycle which plays in favour of the bottoming heat recovery steam generator and the related steam cycle.

Technical background

The liquefaction of NG takes advantage of the different boiling points of methane, ethane and other gases as a way of purifying each substance. A combination of refrigeration and increased pressure allows each gas to be stored and transported conveniently.[10] Liquefaction process requires a significant amount of energy that affects the operating costs and terminal performance.[10–14] According to the advanced liquefaction processes, about 2900 kJ/kg are consumed in the liquefaction process. Most of the energy is dissipated as heat (2070 kJ/kg) with the remaining stored in the LNG (830 kJ/kg). It is estimated that when the LNG is re-gasified to an ambient temperature of 20 °C, approximately 830 kJ/kg per kg of LNG of cold energy can be recovered.[15] Therefore, there are on-going researches exploring solutions for partially recovering the liquefaction energy; these researches mainly look at direct cold energy utilization[16] and power plant performance improvement by internal heat recovery processes.[17]

The BoG represents approximately 0.10–0.15% of the typical LNG tank storage capacity depending on the boundary conditions and the storage technology.[18–20] Prediction of the BoG rate and heat transfer rates[19] is a crucial task for exploring the possible application of BoG recovery systems in the LNG terminals and in the LNG carriers. Different possibilities for handling the BoG have been explored in Spain as reported in Querol et al.[21] Among the proposed solutions (torch, re-condenser, compressor and re-liquefaction plant) the authors in Querol et al.[21] have presented a plant layout for usefully recovering the cold energy available in the BoG mass fraction during the re-gasification process; a combined heat and power (CHP) arrangement was proposed to economically produce electricity by means of the BoG and improvement on the power plant arrangement was proven. Another CHP application by using a topping air Brayton cycle and a bottoming Helium or Nitrogen cycle has been explored in Dispenza et al.;[22,23] the LNG re-gasification cold energy was used to cool down the bottoming cycle working fluid at the condenser. For 80 MW Helium and 60 MW Nitrogen cycle, a net efficiency of approximately 45 and 41% could be achieved, respectively. Also in La Rocca,[24] the benefit of LNG regasification has been demonstrated for an ethane-based power plant cycle showing that for 2b of Stm^3 LNG regasification capacity, it is possible to recover 50 MW and up to 3 MW. The capability of recovering cold energy from the LNG and BoG re-gasification has also been studied for carbon capture and storage, where the benefit in terms of cost avoidance for CO_2 treatment is presented.[25,26] Another study explored the opportunity to exploit the LNG cold energy for a supercritical CO_2 cycle coupled with an air separation unit. The study shows that utilization for LNG cold energy for pre-cooling the compressor inlet temperature brings to about 55% reduction in compressor power consumption.[27] In the same work, another proposed solution is to utilize such a cold energy for cooling down the condenser of the trans-critical CO_2 presented power plant. Another application for the reuse of the LNG cold energy is for waste heat recovery applications such as organic Rankine cycles (ORCs). The possibility of cooling down the working fluid in the condenser by means of the cold energy available from the LNG allows reducing turbine back-pressure; under optimal conditions more than 60% thermal efficiency increase has been proven.[28] A combined cycle consisting of a direct vapour solar ORC and LNG power generation is presented in Rao et al.;[29] the work highlights the benefit of exploiting the LNG cold energy at the condenser thus contributing to improve the exergetic efficiency (from 4% of the baseline configuration to 10% of the LNG option) and to reduce the overall solar collector and heat exchanger surfaces up to 80 and 30%, respectively. On the power generation side, cold energy from regasification in LNG terminals could be utilized to improve performance of CCGT power plants. Both

the intake air conditioning (simple configuration) and the steam cycle condenser cooling down (complex configuration) solutions have been investigated;[30] the results of the investigation have shown significant improvement from 49 up to 55% in the simple configuration and up to 58% in the complex one.

Unlike previously published research, in which the LNG cold energy availability comes from the demand of the regasification terminal, the proposed paper intends to analyse the case in which the amount of the BoG/LNG matches with the required fuel flow rate required by the GT. This means that for small scale GT (<100 MW), the typical BoG daily rate would be sufficient for running the GT at nominal condition, whereas for large scale GT (up to 350 MW), the BoG will have to be integrated with some additional LNG regasification; the improvement in GT performance (power and efficiency), when the cold energy is used to cool down the air intake to the compressor (through internal heat recovery), is assessed and quantified in the current paper.

The proposed solution is typically not adopted for the huge LNG terminals that provide NG to the gas pipelines, when all the required LNG mass flow rate is regasified. Accordingly, the paper shows that practical benefit in terms of plant efficiency and power delivery increase can be achieved by adopting such a BoG regasification configuration. Furthermore, the proven feasibility of this 'technological simple and economical viable' arrangement leads to apply the proposed solution – in a smaller scale – for the shipping traction, where savings in the fuel tank volume occupancy and increase of efficiency play a double role in the cost savings.

Description of the proposed solution

GT engines and related ST CCs are designed to operate at a particular temperature, pressure and relative humidity (RH) in order to maximize power and efficiency.[9,31] In the power generation scenario, in the range of few MW to several hundreds of MW, ambient conditions change continuously thus influencing CCGT performance. This is because compressors and expanders are dynamic machines designed to deal with a well-defined volumetric flow. Thus, for a given volumetric flow rate, power and efficiency depend on the mass flow rate that is operated by the GT. Indeed, higher inlet temperature will result in lower GT power and efficiency, due to density reduction at the compressor stage. Such a density reduction corresponds to an overall inlet mass flow reduction which forces the GT to operate at off-design conditions thus reducing net power and efficiency. For these reasons, some study has been carried out[30] to understand the benefits of conditioning the compressor inlet temperature. Typically, in power plants, the inlet air is conditioned with vapour compression or absorption chillers. The power consumption of these sub-systems is not negligible and has to be taken into consideration in the performance evaluation of the GT and CCGT; hence, the proposed solution which adopts BoG/LNG cold energy would allow drastically reducing the plant complexity (i.e. costs) and power consumption from these sub-systems. Taking into consideration the BoG/LNG thermodynamic properties and the available models for evaluating the BoG rate,[32,33] the proposed alternative solution in this paper is that of using the BoG/LNG cold energy, from −165 °C to ambient temperature of 10–15 °C, thus reducing the GT inlet temperature. This solution could lead to increased performance without the addition of too many extra components and without the need of electricity or heat power to drive vapour compression or absorption chillers, respectively. Typically, the conventional air conditioning systems require higher *capex* due to the additional equipment (e.g. condenser, cooling tower, pumps, valves, etc.), while the proposed solution would substantially reduce the *capex* to few heat exchangers; Figure 1 shows the schematic of the proposed solution.

Development of the power plant simulator

A CCGT power plant consists of many components (e.g. compressor, combustion chamber, expander, exhaust duct, post firing system, etc.). In order to carry out the analysis, a CCGT simulator has been developed to predict the part load performance and therefore the optimal working conditions for the power plant.[34]

Modelling approach and solution strategy

The modelling approach for the GT simulator is based on a finite volume (*FV*) discretization method for each plant component. Each *FV* is defined by boundary surfaces, J and $J+1$. Each component model is a numerical representation of the spatial and time distribution of relevant quantities. In order to lump the relevant quantities (i.e. temperatures, pressures, wok, losses, etc.), on the boundary J and $J+1$ of each *FV*, preliminary two-dimensional, computational fluid dynamic calculations have been performed to generate a database (DB). Thus, the lumped features are reduced to the *FV* central node J_N. As an example, a *shell & tube* heat transfer device (HTD) tube bundle can be divided into *FVs,* each of them comprising a tube row. The heat transfer rate is related to the lumped flow and geometrical features of the tube row by adopting the classical heat transfer model; similar approach is adopted for the other plant components.[9,34,35]

For each volume in the components, the following correlations are determined:

- Governing equations (mass, momentum, energy, entropy[b]);

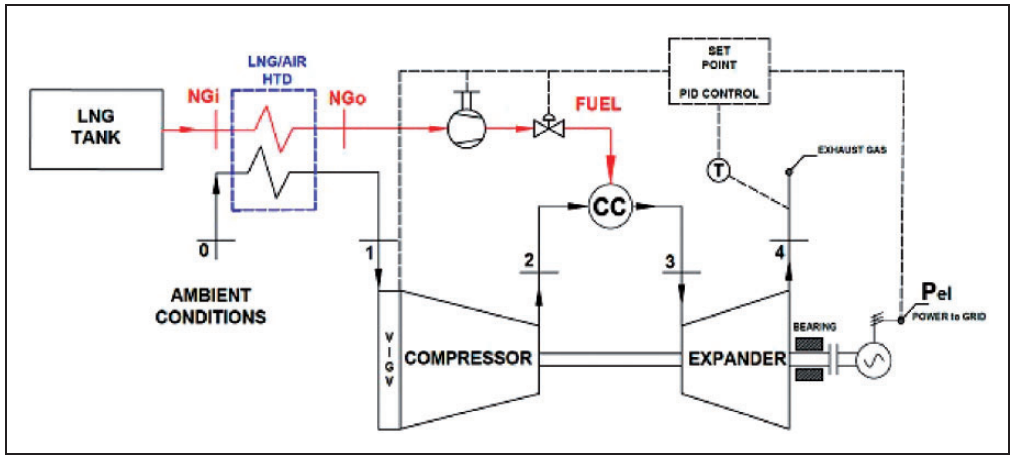

Figure 1. LNG fed gas turbine equipped with compressor air conditioning system.

- Constitutive equations of the system (e.g. fluid properties);
- Auxiliary equations (e.g. eps-NTU heat transfer approach).

The auxiliary equations allow defining the source term of the governing equations establishing the most adequate correlation for the assessment of the pressure loss, heat transfer coefficients and so on. The components and connecting modules are assembled to represent a CCGT power plant. As a result, the physical plant simulator is represented by equation (1)

$$\boldsymbol{F}(\mathbf{g}, \mathbf{z}, \mathbf{d}, \mathbf{rf}, \mathbf{af}) = 0 \tag{1}$$

In order to set the geometrical and thermodynamic limitation for the variables, ensuring the feasibility of the solution, a set of inequalities is established, as in equation (2)

$$\mathbf{D}(\mathbf{g}, \mathbf{z}, \mathbf{d}, \mathbf{rf}, \mathbf{af}) \geqslant 0 \tag{2}$$

in which the vector **g** includes geometric and global quantities, **z** includes process and state quantities (pressures, temperatures, mass flows, fluid compositions, flow angles, rotational velocities, stresses and so on), **d** is the vector for boundary conditions (site pressure, temperature and RH), **rf** is the vector of reality functions (RFs) and **af** is the vector of actuality functions (AFs). An objective function (*ObF*) is established to solve for the unknown quantities, as in equation (3).[34]

$$\begin{aligned} &\text{Minimize } \{ObF | \boldsymbol{F}(\mathbf{g}, \mathbf{z}, \mathbf{d}, \mathbf{rf}, \mathbf{af}) \\ &= 0;\ \mathbf{D}(\mathbf{g}, \mathbf{z}, \mathbf{d}, \mathbf{rf}, \mathbf{af}) \geqslant 0\} \end{aligned} \tag{3}$$

where **z** is the vector of unknown quantities.

*RF*s are introduced to allow the model to reproduce the behaviour of an existing machine in a reference situation (usually new and clean conditions). *AF*s

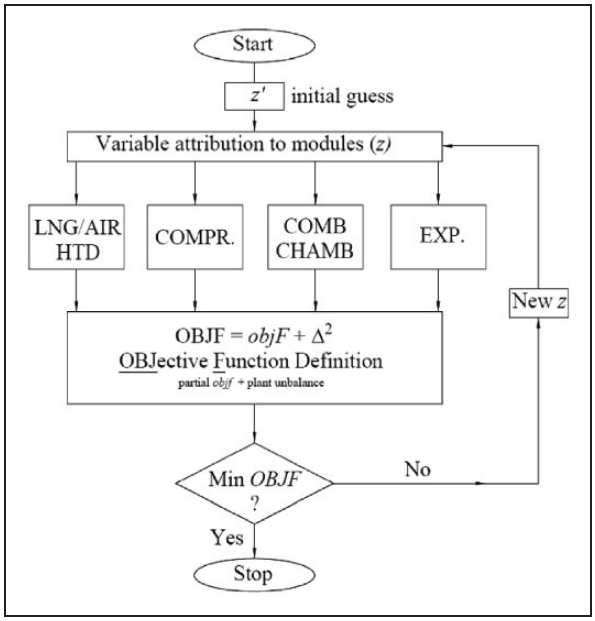

Figure 2. Modular structure calculation method – ECRQP.

are introduced to update the component maps and calculate the actual performance of the component. Indeed during operations, the component behaviour changes continuously due to deterioration related to fouling, erosion, wear and tear. The solution technique is based on a modular approach of elementary component models that calculates processes, fluid properties and machinery features. Figure 2 gives an outline of the modular modelling and the algorithm structure for optimized solution.

Accordingly, a section is dedicated to the distribution to the various component models (modules) of the **g, z, d, rf, af.** Each module performs the dedicated calculations providing a partial $ObF_{j\text{-}th}$ and partial $\Delta_{j\text{-}th}$. A section provides for defining the overall *OBj*F to be minimized. The optimization solution is based on the Equalities Constraints Recursive Quadratic Programming technique and it leads to solve the mathematical formulation of the problem. Optimal solution

is achieved by combining the Lagrange and the penalty functions that allow for robust and fast computational tool; details are given in Cerri.[34]

Methodological approach

Equations and inequalities that describe the components and plant behaviour are addressed to solve different calculations:

- *Cycle calculation*: preliminary calculation where the cycle potential is investigated with only few constraints relating to thermodynamic quantities (typically pressure and temperature). The output of this calculation (mass flow rates, power across different component boundaries and the overall performances) are all thermodynamic quantities in each section of the CCGT power plant;
- *Sizing*: this calculation is for machines and equipment sizing and alternative global parameters to describe their off-design behaviour. Input data are from the cycle calculations or may come from DB related to the commercially available machines and equipment close to the cycle requirements.
- *Off-design analysis*: this analysis requires the knowledge of geometrical data, architecture and some global parameters related to the plant components. The performance maps of the machine and equipment are calculated. Changes in the independent quantities may be investigated according to the control strategy.
- *Matching*: this is the assembling step of the models constituting the simulator, in which component maps are matched together to achieve the whole plant performance; the plant performance can be evaluated for full load and part load operating conditions.

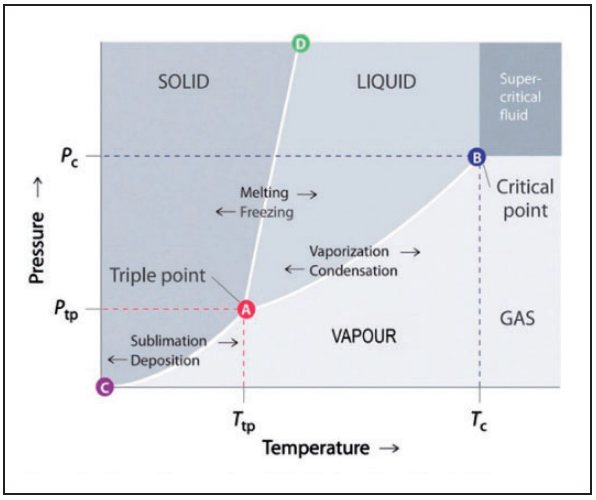

Figure 3. Pressure versus temperature phase chart of a general substance.[36,37]

These calculation steps are performed by means of various optimization techniques based on the quasi Newton algorithms and on genetic algorithms. Details are given in Cerri and Stefano[9] and Cerri.[34]

Phase change in LNG HTD

Working fluid reality. The working fluid (humid air) needs a dedicated physical model, which includes the phase change, sublimation and mass separation into consideration. In the present paper, humid air has been modelled as a mixture of O_2, N_2, CO_2, Ar and H_2O; each characterised by its own thermodynamic properties. The working fluid will reach its dew point (DP) during the heat transfer process between the cold regasified NG stream and the ambient air stream, because of its temperature reduction. DP occurs also when the working fluid pressure, p_{WF}, becomes higher than the saturation point at DP pressure, p_{DP}, and temperature, T_{DP}. Under these conditions, the water vapour becomes liquid and separates from the gas, as shown in Figure 3.

LNG–AIR transfer device. The cooling of the inlet air to the compressor is achieved through the LNG regasification. The heat transfer processes have been modelled by taking into account the fluid phase change and separation phenomena (multi-zone modelling approach). Figure 4 shows the LNG–AIR HTD component model together with the temperature profiles and the thermodynamic quantities. The possibility of achieving the saturation condition (DP in the temperature profiles diagram of Figure 4) for the hot stream has also been taken into consideration in the model. When this condition occurs, some water condensate (WC) mass flow rate is extracted at the exit of the HTD and the overall heat power transferred from the hot stream to the cold stream is divided in two contributions: the first is only related with the sensible heat ($Q_{1\text{-}D}$), the second takes into account the condensing phenomena ($Q_{D\text{-}2}$). The LNG–AIR HTD has been modelled by adopting the ε-NTU approach[9,38] for both sizing and off-design analysis. By solving the sizing calculation, the inlet and outlet temperatures of both the hot and cold stream are established, thus the effectiveness is calculated. A tube bundles heat exchanger has been chosen, and an existing DB with heat transfer and pressure loss coefficients has been used to determine the NTU and S values.[9] Concerning off-design calculations (required also for RFs, AFs identification), the heat transfer coefficients (U) on both sides are evaluated on the bases of reference values as Rohsenow et al.,[38] taking mass flow rate (m), specific heat (c_p), viscosity (μ) and thermal conductivity (λ) into consideration (equation (4))

$$U = U_r \left(\frac{m}{m_R}\right)^a \left(\frac{\mu}{\mu_R}\right)^b \left(\frac{\lambda}{\lambda_R}\right)^c \cdot \left(\frac{c_p}{c_p R}\right)^d \cdot rf \cdot af \qquad (4)$$

a, b, c, d being chosen according to the HTD architecture and heat exchanging media. Pressure losses are evaluated on the basis of the reference value as a function of the actual corrected mass flow μ. Details of the LNG–AIR HTD are given in Appendix 1 – LNG/AIR HTD model.

GT simulator and component model

The generic GT simulator is a tool that incorporates design mode (sizing), surge criteria and loss models. The sizing process has been performed by adopting lumped performance of cascades, HTDs and other components, as described hereafter. The GT simulator has been developed including the main components such as compressor, combustion chamber and expander (including the cooling system).[39–41] Such technologies have been embedded into the component model DB. Accordingly, during the sizing of the GT, the selection of the optimum configuration and geometry has been carried out for the compressor and the expander; the lumping procedure described in section '*Modelling approach and solution strategy*' has been adopted and parameters such as work, losses and heat transfer coefficients have been established for each FV, characterizing the GT blade rows; more information about the simulator have been added in Appendix 2.

Case studies

In this section, two different case studies are presented. The first case study analyses the LNG–AIR HTD component model for demonstrating its capability to predict profile temperatures, WC separation fraction and heat power versus the variability of ambient temperature, RH and LNG/BoG mass fraction. The second case study shows how the conditioning of the air intake to the GT by means of the LNG–AIR HTD brings to increase the power production, the efficiency and therefore the revenues associated for the savings of fuel and for the increase in electric work production.

Model validation: LNG–AIR HTD

The LNG–AIR HTD model has been carried out to assess its behaviour during off-design conditions. The LNG–AIR HTD model description is given in Appendix 1, where thermodynamic quantities, such as temperature, pressure, mass flow rates and heat power transferred from the hot to the cold stream are presented. Table 1 shows the International Organization for Standardization (ISO) ambient conditions, reference temperatures, mass flows and pressures as well as the HTD effectiveness and pressure drop. Starting from the ISO conditions, air mass fraction compositions have been evaluated to establish the fluid properties and the DP conditions, which depend on the amount of H_2O content in the mixture. The air mass fraction composition in the reference condition is made of $O_2 = 0.2312$, $N_2{}^c = 0.7620$, $CO_2 = 0.0005$ and $H_2O = 0.0063$. The influence of ambient temperature change on the HTD performance has been evaluated, for the range of 5–25 °C, as shown in Figure 5. The continuous black line represents the trend of the temperature T_1, if the air is characterized by the ISO condition (humid air), while in case of 0% RH (dry air), the T_1 trend is given by the dashed line.

Below the DP (dashed red line), some fraction of the H_2O changes phase from vapour to liquid, and it

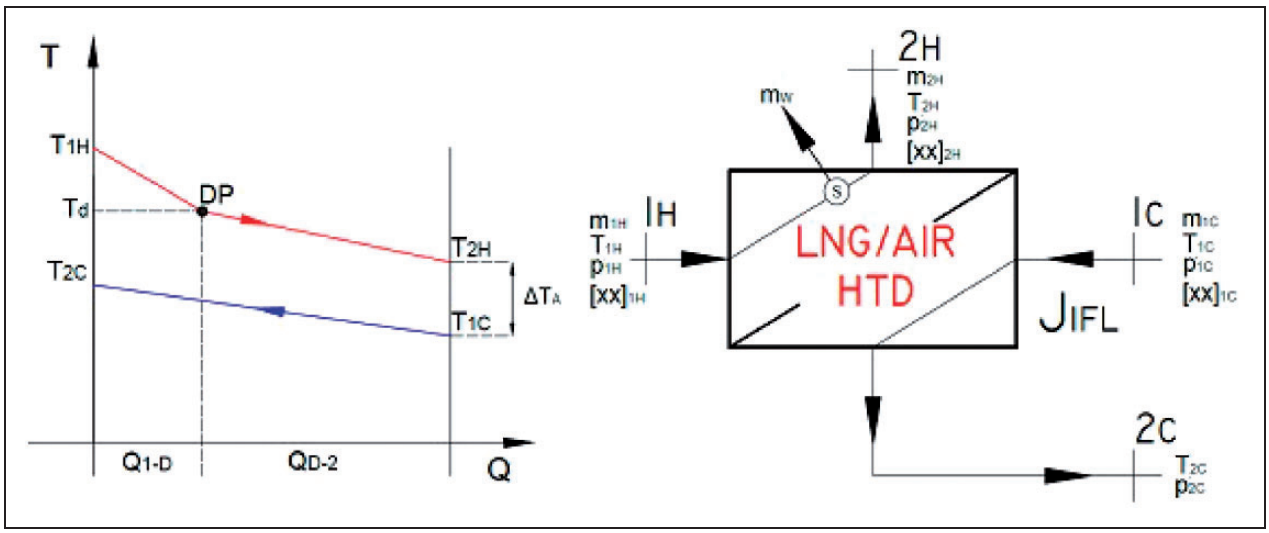

Figure 4. Sketch of the LNG-AIR HTD component model and related temperature profiles.
HTD: heat transfer device; LNG: liquefied natural gas.

Table 1. Ambient conditions, reference data and assumptions.

Ambient conditions – ISO		
p1	101.3	(kPa)
T1	15.0	(°C)
RH	60.0	(%)
Reference data		
TLNGi	−165.0	(°C)
T0	15.0	(°C)
LNG	15.1	(kg/s)
m0	683.7	(kg/s)
pLNGi	150.0	(kPa)
p0	101.3	(kPa)
Assumptions		
ε	90.0	(%)
Δp01	1.0	(%)
ΔpLNG	1.0	(%)

LNG: liquefied natural gas; RH: relative humidity.

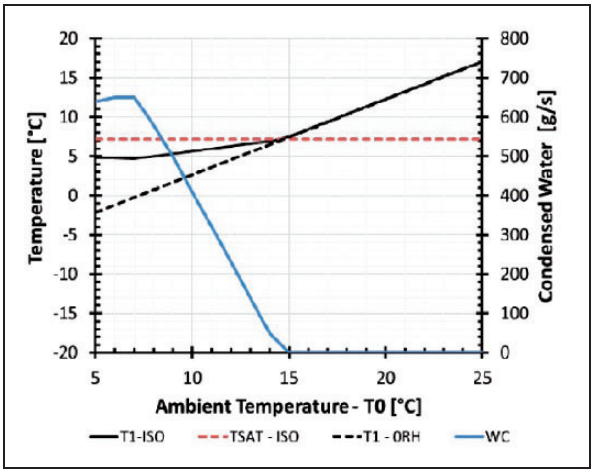

Figure 5. Temperature profiles and condensed water versus ambient temperature for 0%RH and ISO condition.

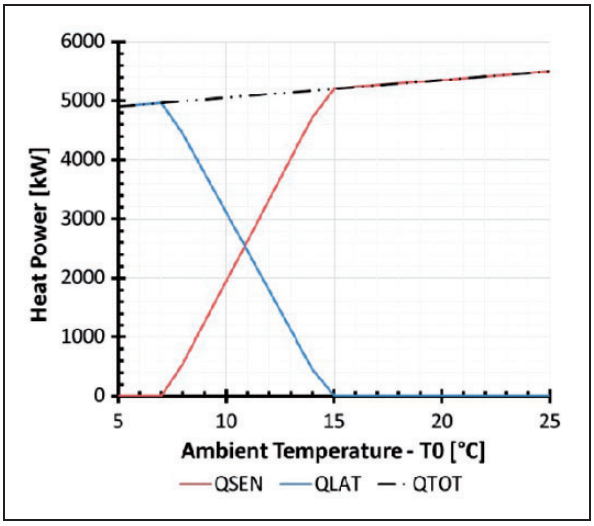

Figure 6. Heat power contribution versus ambient temperature for ISO condition.

brings to the different trends of T_1. Indeed, the temperature reduction in the ISO case is lower if compared to the case with zero RH. In Figure 6, the black dashed line represents the overall heat power (around 5000 kWt) that is exchanged between the two streams, which equals the sum of sensible (Q_{SEN}) and latent heat (Q_{LAT}); on the contrary, when temperatures are higher than the T_{DP} only sensible heat exists (red line). Under a certain temperature, phase change always takes place and the consequent heat transfer process is characterized by the condensing phenomena. In between these temperatures, the HTD deals with a section in which the heat transfer phenomenon is purely sensible and a part with both. In conclusion, the lower the ambient temperature, the higher the condensed water, which for 5 °C is approximately 650 g/s.

The LNG–AIR HTD component model has been used to calculate the change in thermodynamic parameters when LNG/BoG fuel mass flow varies between 0 and 20 kg/s. It is worth noting that such a large variability in LNG mass flow rate usually does not occur in the heavy duty GT-based power plant, but this analysis helps to understand how temperatures, condensed water and heat power vary. Assuming $T_0 = 15\,^{\circ}\mathrm{C}$, RH = 60%, $p_0 = 101.3$ kPa and the reference mass flow rate $m_0 = 683.7$ kg/s, the results from the analysis are shown in Figures 7 and 8. It should be noted that the HTD effectiveness is set at 0.9 for all the evaluation points, under the hypothesis that all are design points. It can be seen in Figure 7 that the higher the LNG mass flow rate, the lower is the hot stream outlet temperature, T_1. Additionally, the water separated from the air mixture increases when the LNG mass flow increases. Figure 8 shows the trend of heat power, showing a quasi linear behaviour with respect to the LNG stream; these evaluations are useful for the analysis of the GT case, where the fuel mass flows change under part load conditions. Variability of RH has been also investigated, being the water content in the air influenced by ambient temperature and RH.

The effects of RH change on parameters of concern are reported in Figures 9 and 10. Evaluations have been performed assuming the reference data of Table 1. In Figure 9, the dashed red line represents the wet bulb temperature corresponding to the dry bulb temperature at 15 °C for different RH rates. The black line (T_1) in Figure 9 shows that the achievement of DP reduces the system's capability to cool down the air mass flow from T_0 to T_1. Additionally, the increase of RH will increase the condensed water, once the DP is achieved. Nevertheless, the LNG

outlet temperature remains practically unchanged (dashed green line). By taking the heat transferred into account, Figure 10 shows that the overall amount of heat power is related with the sensible heat power, red line, when the RH is lower than that of the DP. Meanwhile when the RH is between 60 and 100%, the heat transfer process is characterized by latent and sensible heat. During the setup of the model, psychometric chart together with REFPROP software[42] has been adopted for validating the output of the calculations. DP temperatures as well as WC mass have been checked. According to the HTD modelling approach based on the ε-NTU method, where phase change phenomena take place, the authors have validated the HTD in previous work.[9]

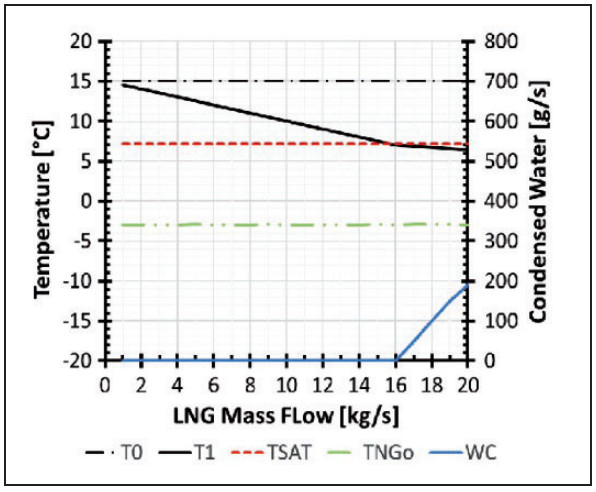

Figure 7. Temperature profiles and condensed water versus LNG mass flow rate at ISO condition.
LNG: liquefied natural gas; WC: condensed water.

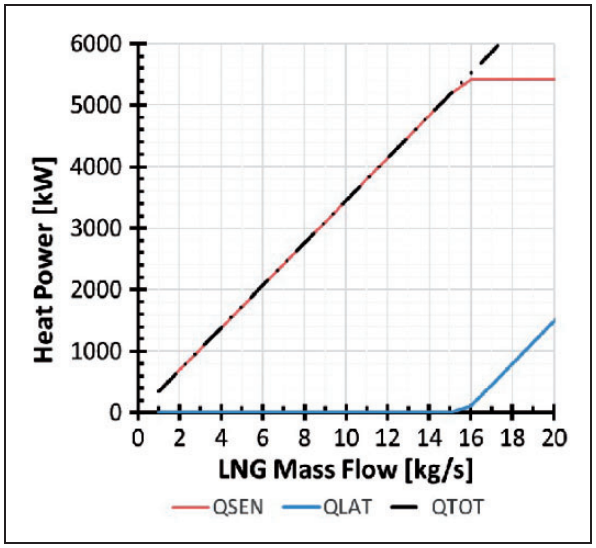

Figure 8. Heat power contribution versus LNG mass flow rate at ISO condition.
LNG: liquefied natural gas.

Case study: 300 MW F class GT LNG fed power plant

The LNG–AIR HTD has been considered for a 300 MW F class GT in which the cold from the BoG and LNG regasification is considered. The generic 300 MW F class GT simulator has been validated with data published by the GT OEM.[43] More details on the validation of the simulator are given in Cerri et al.;[31,35] the main validation results are shown in Figure 11 (blue triangles for power, red squares for efficiency). In Figure 11, one can see the ratio between the machine actual power and actual efficiency and the nominal values, varying the compressor inlet temperature. It can be remarked that the calculated values

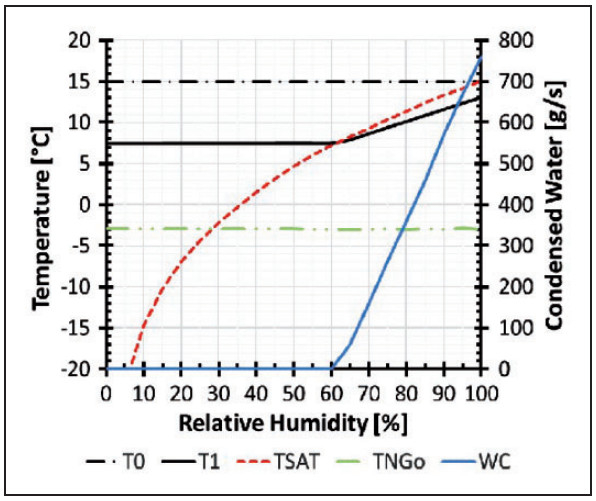

Figure 9. Temperature profiles and condensed water versus RH.
WC: condensed water.

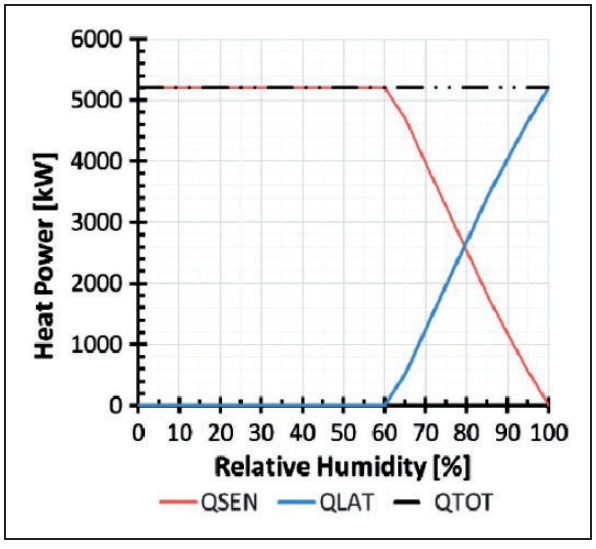

Figure 10. Temperature profiles and condensed water versus RH.

(blue triangles for power and red squares for efficiency) fit very well with the data obtained from the GT manufacturer – the continuous green and grey lines representing non-dimensional power and efficiency, respectively.

The simulator with re-gasified LNG was built based on the validated simulator and it has been matched to the LNG–AIR HTD. Figures 12 and 13 show the comparisons between the baseline GT (CASE#0 – blue lines – no air inlet cooling) and the cooled inlet air from the re-gasified LNG (CASE#1 – red line – with air inlet cooling). Electric power, fuel mass flow and compressor inlet temperatures are presented in Figure 12; in Figure 13, variable inlet guide vanes (VIGV) and efficiency are given for different ambient temperatures. From Figure 12, it can be seen that the compressor inlet temperature for CASE#0 and CASE#1 reduces when conditioned through the LNG–AIR HTD; lower compressor inlet temperature results in higher operational mass flow rate for the GT. As a consequence, the generated power (continuous lines) increases (red line) and the fuel consumption increases as well (dotted line). However, one can notice that the increase of generated power is higher than the increase of fuel consumption; hence, the GT efficiency increases if compared with the baseline. Figure 13 shows that different PID strategies were used for VIGV control in the CASE#0 and CASE#1, in order to achieve the system level outputs. Due to the reduction of inlet temperature, the VIGV have to deal with – for a given mass flow rate – with a lower volumetric flow. Consequently, for the same ambient temperature, the CASE #1 shows how the VIGV opening is lower.

A preliminary economic analysis has been conducted for the GT – LNG–AIR HTD configuration. However, a typical cost benefit analysis is not performed because the *capex* and *opex* of the additional HTD are not embedded in the simulator. This preliminary economic evaluation has been carried out using a typical Mediterranean Costal Area hourly temperature diagram over a year. Based on Figures 12 and 13, the generated electric work and the fuel consumption are integrated over the year to obtain the annual electric work and the fuel mass consumption. In order to establish the income related to electricity production,

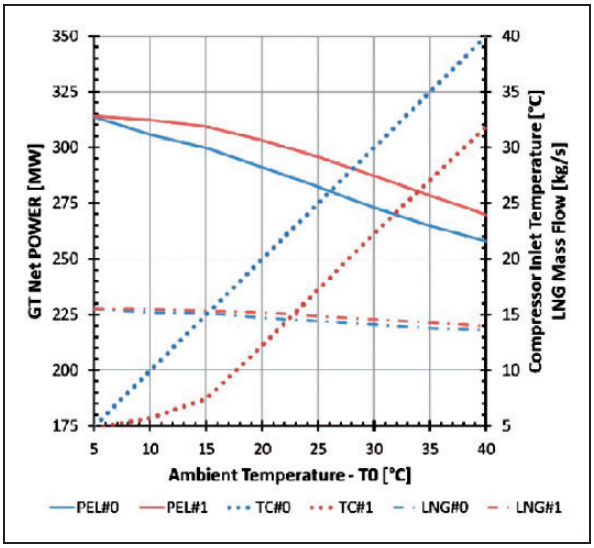

Figure 12. Power output, fuel consumption and compressor inlet temperature versus ambient temperature CASE#0 and CASE#1.
LNG: liquefied natural gas.

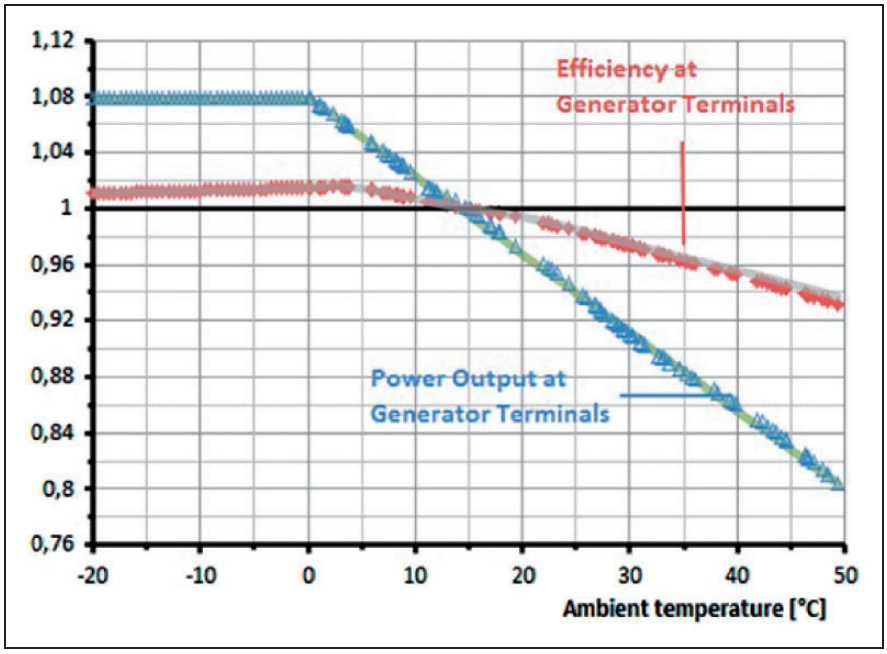

Figure 11. Generic 300 MW F class GT simulator versus real machine behaviour – power and efficiency.[43]

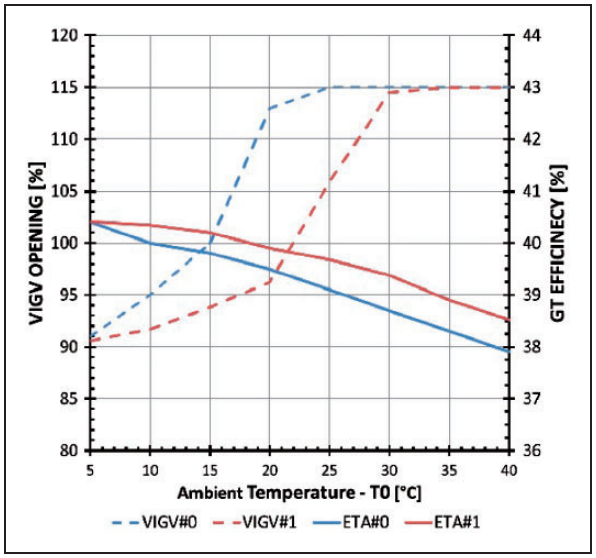

Figure 13. Variable inlet guide vane (VIGV) opening and GT efficiency versus ambient temperature CASE#0 and CASE#1. ETA: efficiency.

a selling price of 5 c€/kWh has been assumed. Price of LNG has been assumed to be 20 c€/Nm^3. Equation (5) represents the income related to the higher power generated in the CASE#1 minus that of the reference case. Equation (6) represents the cost increase for the higher fuel mass consumption and finally equation (7) represents the difference between the two terms, which is the *GAIN*.

$$\Delta_{WORK} = \int_0^{8760} P1_{el}(t) \cdot €_{el}(t) \cdot dt - \int_0^{8760} P0_{el}(t) \cdot €_{el}(t) \cdot \mathrm{d}t \tag{5}$$

$$\Delta_{fuel} = \int_0^{8760} m1_{fuel}(t) \cdot €_{fuel}(t) \cdot \mathrm{d}t - \int_0^{8760} m0_{fuel}(t) \cdot €_{fuel}(t) \cdot \mathrm{d}t \tag{6}$$

$$GAIN = \Delta_{WORK} - \Delta_{fuel} \tag{7}$$

Figure 14 summarises the preliminary economic analysis for the power plant fed with re-gasified LNG. The red line represents the ambient temperature distribution along the year (8760 h). The continuous black line represents the income related to the increase of electric work. Meanwhile, the dotted black line is the cost for the increased fuel mass. The net *GAIN* as defined in equation (7) is shown by the continuous blue line. Assuming the temperature distribution given in Figure 14, the integral over a year could yield a gain of 650,000€ compared to the baseline. Such a yearly gain it purely theoretical, indeed it has to be remarked that in the real CCGT power plant, according to the various maintenance issues and to possible power shut down, the CCGT utilization factor is approximately about 90-95%. The yearly gain thus assumes a values of 600,000€.

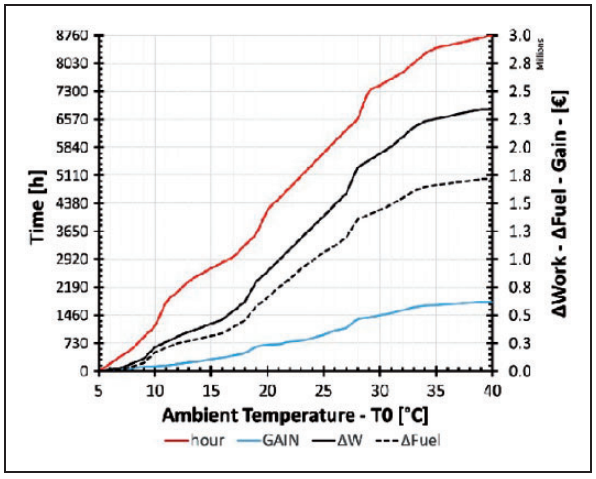

Figure 14. Yearly ambient temperature distribution and related electric work, fuel consumption and gain, expressed in M€.

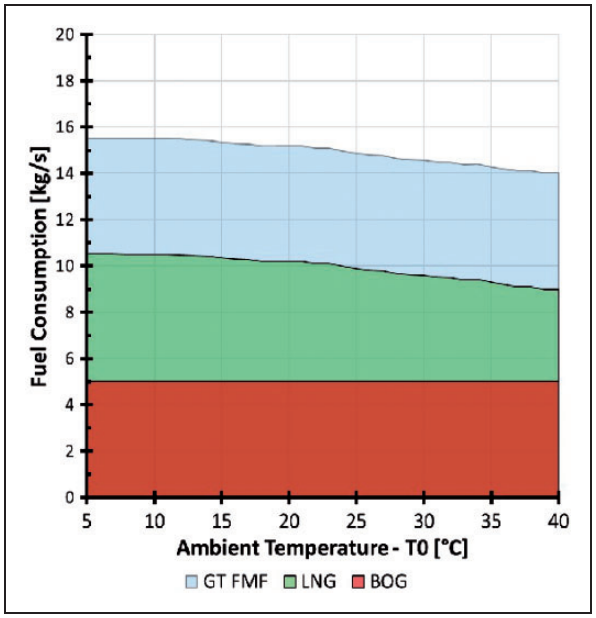

Figure 15. Fuel mass flow, BoG availability and extra LNG. BoG: boil-off gas; FMF: fuel mass flow rate; GT: gas turbine; LNG: liquefied natural gas.

Another consideration is related to the daily amount of BoG and the fuel mass flow rate required to feed the GT. According to the available data,[44] the assumption of 5 kg/s BoG coupled with the hypothesis that such a BoG is constant over the time in Figure 15 the GT fuel consumption, the BoG flow rate and the additional LNG mass flow rate required to match the GT fuel consumption are presented versus the ambient temperature. It means that for a 300 MW GT, the terminal BoG daily rate is not sufficient for ensuring the GT operation. Surely, if the power plant size is of 100 MW, such a BoG rate will totally match the GT requirement.

Conclusions

This paper demonstrates one possibility for recovering part of the energy used for LNG liquefaction during the regasification phase. The proposed methodology contributes directly to the effort to increase LNG. Naturally, a 0.15% BoG spontaneously re-gasifies from the LNG tanks in the terminal or in the LNG carrier, which essentially provides availability of cold energy. The paper has explored the solution of conditioning the GT inlet temperature, by utilizing the cold energy coming from the BoG. In order to recover such a cold energy, a dedicated HTD component model (LNG–AIR HTD) including phase change phenomena and water separation has been developed. Thermodynamic analyses on the LNG–AIR HTD have been carried out, showing the influence of operating parameters such as ambient temperature and RH on the heat transfer process. Then, the possibility of directly feeding a CCGT with such BoG fraction has been explored. A 300 MW F class GT simulator, which has been validated with available OEM data, was used for this study. For a given ambient temperature variability over a year, the simulator has been used to evaluate the increase in electricity production and in efficiency that showed a revenue of 600,000€/year, due to the BoG cold energy recovery. It has to be noted that the revenue increase does not take into account the *capex* and *opex* of the dedicated HTD and the control system for LNG fuel feeding – detailed cost-benefit analyses are not shown in this paper. Nevertheless, the focus here is to highlight that cold energy with LNG–AIR HTD could be used in a 300 MW F class GT resulting in higher revenue. Furthermore, for CCGT power plant, the bottoming cycle will be positively influenced by the increase of mass flow rate due to conditioning of the intake duct air. Looking forward, this could be an interesting solution for LNG carriers, where the typical power demand is approximately 30–40 MW, where the daily BoG rate matches the GT fuel requirements.[44] In these applications, no additional fuel would be required, increasing performance, the storage capacity of the LNG carrier and substantially making 'free' the transportation of the cargo. The next step for this piece of work will be performance evaluation of the CCGT power plant cycle fed by LNG coupled with an accurate cost benefit analysis – in order to demonstrate the pay-back period and the increase in the net present value.

Declaration of Conflicting Interests

The author(s) declared no potential conflicts of interest with respect to the research, authorship and/or publication of this article.

Funding

The author(s) disclosed receipt of the following financial support for the research, authorship and/or publication of this article: This research was supported by the National Research Foundation, Prime Minister's Office, Singapore under its Energy NIC grant (NRF Award No.: NRF-ENIC-SERTD-SMES-NTUJTCI3C-2016). Acknowledgment also goes to Malaysian Ministry of Higher Education and Universiti Teknologi Malaysia for the research grant VOT 4L174.

Notes

a. Natural gas is stored in liquefied form at around −160 °C.
b. The conservation of entropy for a steady-state open thermodynamic system bounded by a fixed border states: the entropy of the system does not change with the time so that the sum of the entropy convected into the system by the incoming flow, the entropy increase due to external heat fluxes and the entropy produced by internal irreversibility is equal to the entropy extracted by the flow leaving the system. For a non-steady-state thermodynamic process, the conservation law leads to a time differential equation that takes the rate of entropy accumulation inside the system equal to the above entropy fluxes (inlet flows, outlet flows, heat fluxes and internal entropy production).
c. Nitrogen refers to the atmospheric nitrogen whose molecular weight is higher than the pure N_2 because of the other inert gas content (e.g. Argon).

ORCID iD

Alessandro Romagnoli http://orcid.org/0000-0003-1271-5479

References

1. Tergin D. Ensuring energy security. *Foreign Aff* 2006; 85: 69. doi:10.2307/20031912.
2. Lesbirel SH. Diversification and energy security risks: the Japanese case. *Jpn J Polit Sci* 2004; 5: 1–22. doi:10.1017/S146810990400129X.
3. Vivoda V. Diversification of oil import sources and energy security: a key strategy or an elusive objective? *Energ Pol* 2009; 37: 4615–4623. doi:10.1016/j.enpol.2009.06.007.
4. Id U (ExxonMobile). The outlook for energy: a view to 2040. 2016; 1–16. http://corporate.exxonmobil.com/en/energy/energy-outlook/a-view-to-2040.
5. Aleklett K, Höök M, Jakobsson K, et al. The peak of the oil age – analyzing the world oil production reference scenario in World Energy Outlook 2008. *Energ Pol* 2010; 38: 1398–1414. doi:10.1016/j.enpol.2009.11.021.
6. Kumar S, Kwon HT, Choi KH, et al. LNG: an eco-friendly cryogenic fuel for sustainable development. *Appl Energ* 2011; 88: 4264–4273. doi:10.1016/j.apenergy.2011.06.035.
7. Shiva SS and Ashouri N. Minimize evaporation losses by calculating boiloff gas in LPG storage tanks n.d., www.gasprocessingnews.com/features/201602/minimize-evaporation-losses-by-calculating-boiloff-gas-in-lpg-storage-tanks.aspx.
8. Agarwal R and Babaie M. LNG regasification – technology evaluation and cold energy utilisation. *IGT Int Liq Nat Gas Conf Proc* 2013; 3: 2134–2142.
9. Cerri G and Stefano SCM. Steam cycle simulator for CHP plants. *ASME Turbo Expo*, San Antonio, Texas, USA, 3–7 June 2013.
10. Mokhatab S, John M, Jaleel V, et al. *Handbook of liquefied natural gas*. 1st ed. Elsevier, 2013.

11. Songhurst B. LNG plant cost escalation. *Oxf Inst Energy Stud,* Copyright © 2014*;* 8–10.
12. Gas Strategies Group Limited. The outlook for LNG in 2016. 2016: 1–10. http://www.gasstrategies.com/sites/default/files/download/outlook_for_2016_-_gas_strategies.pdf.
13. TECHNIP-COFLEX. LNG plant pricing consideration, 2016. www.technip.com/en.
14. Levine S. Risk and opportunity in a changing world 2016, LNG and renewable power, Le Brattle Group.
15. Franco A and Casarosa C. Thermodynamic and heat transfer analysis of LNG energy recovery for power production. *J Phys Conf Ser* 2014; 547: 12012. doi:10.1088/1742-6596/547/1/012012.
16. Sayyaadi H and Babaelahi M. Thermoeconomic optimization of a cryogenic refrigeration cycle for re-liquefaction of the LNG boil-off gas. *Int J Refrig* 2010; 33: 1197–1207. doi:10.1016/j.ijrefrig.2010.03.008.
17. Dobrota D, Lalić B and Komar I. Problem of boil-off in LNG supply chain. *Trans Marit Sci* 2013; 2: 91–100. doi:10.7225/toms.v02.n02.001.
18. Wordu AA and Peterside B. Estimation of boil-off-gas BOG from refrigerated vessels in liquefied natural gas plant. *Int J Eng Technol* 2013; 3: 44–49.
19. Miana M, Legorburo R, Díez D, et al. Calculation of boil-off rate of liquefied natural gas in mark III tanks of ship carriers by numerical analysis. *Appl Therm Eng* 2016; 93: 279–296. doi:10.1016/j.applthermaleng.2015.09.112.
20. Adom E, Islam SZ and Ji X. Modelling of boil-off gas in LNG tanks: a case study. *Int J Eng Technol* 2010; 2: 292–296.
21. Querol E, Gonzalez-Regueral B, García-Torrent J, et al. Boil off gas (BOG) management in Spanish liquid natural gas (LNG) terminals. *Appl Energ* 2010; 87: 3384–3392. doi:10.1016/j.apenergy.2010.04.021.
22. Dispenza C, Dispenza G, La Rocca V, et al. Exergy recovery during LNG regasification: electric energy production – Part one. *Appl Therm Eng* 2009; 29: 380–387. doi:10.1016/j.applthermaleng.2008.03.036.
23. Dispenza C, Dispenza G, La Rocca V, et al. Exergy recovery during LNG regasification: electric energy production – Part two. *Appl Therm Eng* 2009; 29: 380–387. doi:10.1016/j.applthermaleng.2008.03.036.
24. La Rocca V. Cold recovery during regasification of LNG part one: cold utilization far from the regasification facility. *Energy* 2010; 35: 2049–2058. doi:10.1016/j.energy.2010.01.022.
25. Tuinier MJ, Hamers HP and Van Sint AM. Techno-economic evaluation of cryogenic CO2 capture – a comparison with absorption and membrane technology. *Int J Greenh Gas Contr* 2011; 5: 1559–1565. doi:10.1016/j.ijggc.2011.08.013.
26. Zhang N, Lior N, Liu M, et al. COOLCEP (cool clean efficient power): a novel CO2-capturing oxy-fuel power system with LNG (liquefied natural gas) coldness energy utilization. *Energy* 2010; 35: 1200–1210. doi:10.1016/j.energy.2009.04.002.
27. Mehrpooya M, Kalhorzadeh M and Chahartaghi M. Investigation of novel integrated air separation processes, cold energy recovery of liquefied natural gas and carbon dioxide power cycle. *J Clean Prod* 2016; 113: 411–425. doi:10.1016/j.jclepro.2015.12.058.
28. Liu Y and Guo K. A novel cryogenic power cycle for LNG cold energy recovery. *Energy* 2011; 36: 2828–2833. doi:10.1016/j.energy.2011.02.024.
29. Rao WJ, Zhao LJ, Liu C, et al. A combined cycle utilizing LNG and low-temperature solar energy. *Appl Therm Eng* 2013; 60: 51–60. doi:10.1016/j.applthermaleng.2013.06.043.
30. Stradioto DA, Seelig MF and Schneider PS. Reprint of: performance analysis of a CCGT power plant integrated to a LNG regasification process. *J Nat Gas Sci Eng* 2015; 27: 18–22. doi:10.1016/j.jngse.2015.06.009.
31. Cerri G, Mazzoni S, Giovannelli A, et al. Model of a generic 300 MW F gas turbine for IGCC. *Int Gas Turbine Congr,* Tokyo, Japan 2015.
32. Nasrifar K and Bolland O. Prediction of thermodynamic properties of natural gas mixtures using 10 equations of state including a new cubic two-constant equation of state. *J Pet Sci Eng* 2006; 51: 253–266. doi:10.1016/j.petrol.2006.01.004.
33. Dimopoulos GGG and Frangopoulos CA. A dynamic model for liquefied natural gas evaporation during marine transportation, during marine transportation. Architecture. *Int J Therm* 2008; 11: 123–131.
34. Cerri G. A Simultaneous solution method based on modular approach for power plant analyses and optimized designs and operations. *96-GT-302*: 1–13. Birmingham, UK: ASME.
35. Cerri G, Chennaoui L, Giovannelli A, et al. Expander models for a generic 300 MW f class gas turbine for igcc. *ASME Turbo Expo* 2014; 1–10.
36. http://2012books.lardbucket.org/books/principles-of-general-chemistry-v1.0/s15-07-phase-diagrams.html n.d.
37. Meyers CH, Cragoe CS and Mueller EF. Table and Mollier chart of the thermodynamic properties of 1, 3-butadiene. *J Res Natl Bur Stand (1934)* 1947; 39: 507. doi:10.6028/jres.039.035.
38. Rohsenow WM, Hartnett JP and Cho YI. *Handbook of heat transfer*. vol. 18. McGrow Hill, 1998.
39. Mazzoni S and Cerri G. 'Preliminary turbine cooling requirements'. H2-IGCC deliverable 3.3.4, Roma Tre University, Department of engineering, Rome: Italy, 2013.
40. Han J, Dutta S, Ekkad S. Gas Turbine Heat Transfer and Cooling Technology, 2nd ed., 2012. Boca Raton: CRC Press.
41. Cerri G and Chennaoui L. General method for the development of gas turbine based plant simulators: an IGCC application. ASME TurboExpo 2013, GT2013-94040, Texas, USA.
42. REFPROP. n.d., www.nist.gov/srd/refprop.
43. Siemens. Siemens gas turbine SGT6-5000F. 2008. www.siemens.com.
44. El-Gohary MM. The future of natural gas as a fuel in marine gas turbine for LNG carriers. *Proc Inst Mech Eng Part M J Eng Marit Environ* 2012; 226: 371–377. doi:10.1177/1475090212441444.
45. Cerri G, Salvini C, Procacci R, et al. Fouling and air bleed extracted flow influence on compressor performance, 93 - GT- 366, Copyright © 1993 by ASME.
46. Albeirutty MH, Alghamdi AS and Najjar YS. Heat transfer analysis for a multistage gas turbine using different blade-cooling schemes. *Appl Therm Eng* 2004; 24: 563–577. doi:10.1016/j.applthermaleng.2003.10.007.

47. Boyce MP. *Gas turbine engineering handbook*. Elsevier, 2012.
48. Cohen H, Rogers GFC and Saravanamuttoo HIH. *Gas turbine theory*. 3rd ed. New York: Longman Scientific & Technical, 1987.
49. Logan E and Roy R. *Handbook of turbomachinery*. 2003. Boca Raton: CRC Press. doi:10.1201/9780203911990.
50. Kumar S and Singh O. Thermodynamic evaluation of different gas turbine blade cooling techniques,thermal issues in emerging technologies, ThETA 2, Cairo, Egypt, 17–20 December 2008.
51. Jonsson M, Bolland O, Bücker D, et al. Gas turbine cooling model for evaluation of novel cycles. *ECOS Conference,* Norway 2005; 641–650.

Appendix

Notation

af	array of actuality functions
BoG	boil-off gas
CC	combined cycle, combustion chamber
CCGT	combined cycle gas turbine
CFD	computational fluid dynamic
CHP	combined heat and power
Cp	specific heat capacity
D, d	array of inequality constrains, array of data and boundaries
DB	data base
DOF	degree of freedom
DP	dew point
ECRQP	equalities constraints recursive quadratic programming
ETA	efficiency
€	cost/price
F	array of equality constrains
FV	finite volume
g	array of geometrical and global quantities
ge	equality constraint
gi	inequality constraint
GA	genetic algorithm
GT	gas turbine
HTD	heat transfer device
J	mathematical index
LHV	low heating value
LNG	liquefied natural gas
m	mass flow rate
NG	natural gas
NTU	number of heat transfer unit
ObF	objective function
ORC	organic Rankine cycle
P	power
p	pressure
PES	primary energy source
PID	proportional integral derivative
Q	heat power
rf	array of reality functions
RH	relative humidity
ST	steam turbine
T	temperature
U	heat transfer coefficient
VIGV	variable inlet guide vanes
[xx]	gas composition
W	work
WC	condensed water
z	array of unknowns, knowns and degrees of freedom

Greek symbols

ε	effectiveness
δ	deviation
λ	thermal conductivity
μ	dynamic viscosity
Δ	difference, unbalance

Subscripts

0, 1, 2,.., N	station number
C	cold stream
DP	dew point
EL	electric
FMF	fuel mass flow rate
H	hot stream
i	inlet
LAT	latent
o	outlet
R	reference quantity
SAT	saturation
SEN	sensible
TOT	overall, total
WF	working fluid

Appendix 1. LNG HTD model

The outlet temperature on the hot stream is related to the inlet temperature of the cold fluid and on the minimum temperature difference ΔT_A (also the effectiveness could be adopted, the approach does not change)

$$T_{2Hc} = T_{1c} + \Delta T_A \tag{1}$$

or

$$\varepsilon = \frac{T_{1H} - T_{1C}}{T_{1H} - T_{2H}} \tag{2}$$

Following the hot stream, the pressure losses Δp_H are taken in the model into account

$$p_{2Hc} = p_{1H} \cdot \left(1 - \frac{\Delta p_H}{100}\right) \tag{3}$$

By means of the constitutive equations, the fluid properties can be established in the section $1H$

$$c_{p1H} = f(T_{1H}, p_{1H}, [xx]_{1H}) \tag{4}$$

$$h_{1H} = f(T_{1H}, p_{1H}, [xx]_{1H}) \tag{5}$$

At this point, a check is performed on the possibility that the dew point is achieved. Thus, the dew point thermodynamic quantities (saturation temperature, enthalpy and partial pressure) are evaluated by the dedicated subroutine.

$$(T, p_v, h)\big|_{Dew} = f(p_{1H}, [xx]_{1H}) \tag{6}$$

If the dew point temperature is higher than the outlet temperature, condensing phenomena take place ($kSEP = 1$). If not ($kSEP = 0$), the outlet mass flow rate and composition are the same of that of the inlet, and the outlet conditions can be established by means of the constitutive equations.

$$IF\ T_D \geqslant T_{2H} \rightarrow kSEP = 1 \tag{7}$$

$$IF\ T_D < T_{2H} \rightarrow kSEP = 0 \tag{8}$$

In the case that $kSEP = 1$, the properties of the biphase mixture are established for the pressure p_{1H} and the temperature T_{Dew} (point D) and for the conditions of the point $2H$, characterized the pressure p_{2H} and the temperature T_{2H}.

$$h_{1H} = f(p_{1H}, T_{1H}, [xx]_{1H}) \tag{9}$$

$$h_{Dew} = f(p_{1H}, [xx]_{1H}) \tag{10}$$

$$T_{Dew} = f(p_{1H}, [xx]_{1H}) \tag{11}$$

$$p_{Dew} = f(p_v, [xx]_{1H}) \tag{12}$$

Specific heat of the hot side inlet temperature is calculated by means of equation (20), while subroutine GSTHPRM also calculates outlet stream composition (equation (21)) that allows to define the thermodynamic properties of the outlet stream.

$$c_{pDew} = f(p_{1H}, T_{Dew}, [xx]_{1H}) \tag{13}$$

$$[xx]_{2H} = f(p_{2H}, T_{2H}) \tag{14}$$

$$c_{p2H} = f(p_{2H}, T_{2H}, [xx]_{2H}) \tag{15}$$

$$c_{pD2} = (c_{pDew} + c_{p2}) \cdot 0.5 \tag{16}$$

Heat exchanged can be calculated by means of equations (24) and (25)

$$Q_{1-D} = m_{1H} \cdot (h_{1H} - h_{Dew}) \tag{17}$$

$$Q_{D-2} = m_1 \cdot c_{pD2}(T_{Dew} - T_{2H}) \tag{18}$$

$$Q_H = Q_{1-D} + Q_{D-2} \tag{19}$$

$$m_{2H} = m_{1H} - m_{cond} \tag{20}$$

Being m_{cond} the condensed water mass flow established as function of

$$m_{cond} = f(p_2, T_2) \tag{21}$$

In the case that $kSEP = 0$, mono-phase fluid properties are established as follows

$$h_{2H} = f(p_{2H}, T_{2H}, [xx]_{1H}) \tag{22}$$

$$m_{2H} = m_{1H} \tag{23}$$

$$[xx]_{1H} = [xx]_{2H} \tag{24}$$

$$Q_H = m_{1H} \cdot (h_{1H} - h_{2H}) \tag{25}$$

Hot side outlet stream temperature and pressure are calculated by means of

$$T_{2Hc} = T_{1C} + \Delta T_A \tag{26}$$

$$p_{2Hc} = p_{1H} \cdot \left(1 - \frac{\Delta p_H}{100}\right) \tag{27}$$

Thermodynamic properties of the cold side stream are obtained by means of the following equations

$$Q_C = m_{1C} \cdot (h_{2C} - h_{1C}) \tag{28}$$

$$h_{2Cc} = h_{1C} + \frac{Q_C}{m_{1C}} \tag{29}$$

$$h_{1C} = f(p_{1C}, T_{1C}, [xx]_{1C}) \tag{30}$$

$$h_{2C} = f(p_{2C}, T_{2C}, [xx]_{1C}) \tag{31}$$

$$p_{2Cc} = p_{1C} \cdot \left(1 - \frac{\Delta p_C}{100}\right) \tag{32}$$

Equality constraints

$$ge_I(1) = p_{2Cc} - p_{2C} \tag{33}$$

$$ge_I(2) = p_{2Hc} - p_{2H} \tag{34}$$

$$ge_I(3) = h_{2Cc} - h_{2C} \tag{35}$$

$$ge_I(4) = T_{2Hc} - T_{2H} \tag{36}$$

Inequality constraints

$$gi_I(1) = T_{1H} - T_{2H} \tag{37}$$

$$gi_I(2) = T_{2C} - T_{1C} \quad (38)$$

$$gi_I(3) = T_H - T_{2C} \quad (39)$$

$$gi_I(4) = T_{2H} - T_{1C} \quad (40)$$

The decision variables of the intercooler component model are summarized:

Decision variables

$$x_I(1) = p_{2C} \quad (41)$$

$$x_I(2) = p_{2H} \quad (42)$$

$$x_I(3) = T_{2C} \quad (43)$$

$$x_I(4) = T_{2H} \quad (44)$$

Input

1. m_{1H} *(kg/s)* hot inlet mass flow
2. T_{1H} *(K)* hot stream inlet temperature
3. p_{1H} *(kPa)* hot stream inlet pressure
4. T_{2H} *(K)* hot stream outlet temperature
5. p_{2H} *(kPa)* hot stream outlet pressure
6. T_{2C} *(K)* cold stream outlet temperature
7. p_{2C} *(kPa)* cold stream outlet pressure
8. $[xx]_{1H}$ *[-]*$_m$ hot stream inlet mass fraction composition (O_2, N_2, CO_2, H_2O)
9. m_{1C} *(kg/s)* cold inlet mass flow
10. T_{1C} *(K)* cold stream inlet temperature
11. p_{1C} *(kPa)* cold stream inlet pressure
12. Δp_H *(%)* AIR side pressure losses
13. Δp_C *(%)* LNG side pressure losses
14. ΔT_A *(K)* approach temperatures or effectiveness
15. *Eps [-]* effectiveness or approach temperature
16. $[xx]_{3C}$ *[-]*$_m$ cold stream inlet mass fraction composition (O_2, N_2, CO_2, H_2O)

Output

1. m_{2H} *(kg/s)* hot stream outlet mass flow
2. m_{Cond} *(kg/s)* hot stream mass flow condensed and separated
3. T_{Dew} *(K)* absolute saturation temperature of the hot stream
4. $Q_{1\text{-}D}$ *(kJ/kg)* sensible heat
5. $Q_{D\text{-}2}$ *(kJ/kg)* sensible heat and latent heat
6. Q_H *(kJ/kg)* heat power removed from the system
7. $[xx]_{2H}$ *[-]*$_m$ hot stream outlet mass fraction composition (O_2, N_2, CO_2, H_2O)
8. ge_{HTD} *[-]* equality constraint array
9. gi_{HTD} *[-]* inequality constraint array
10. Δe_{HTD} *[-]* LNG-AIR unbalance
11. ff_{HTD} *[-]* LNG-AIR objective function (e.g. cost)

Appendix 2. Gas turbine component models

Compressor

Compressor thermodynamic and fluid-dynamic quantities are evaluated at the exit of each blade row and they are combined for stack cumulative contribution.[45] Work transfer is evaluated by considering the losses in a global manner. Such losses are correlated with the inlet incidence flow angle and exit deviation (δ). Profile losses on the blade surfaces, skin friction losses on the annulus walls and secondary losses are taken into account using various empirical correlations available in the literature.[45]

Expander

The gas coming from the combustion chamber (CC) has been treated as a zero dimensional model in which performances are lumped. The model takes the combustion products, pressure losses and the pollutants into account and the different coolant flows bleed from the compressor entering the expander in different stations. The turbine cooling has been modelled in the expander by taking into account additional losses related with various aspects (momentum conservation, heat transfer process and mixing).

Gas turbine cooling

Gas turbine cooling systems can be seen as a complex arrangement of series and parallel heat transfer devices. In the development of the Cooling Component, various heat transfer phenomena have to be taken into consideration to properly design the cooling system.[35,40,46–51] The simulator takes an expander cooling lumped model into account, which implies transfer of heat from the main flow (hot gas) to the coolant flows. In such a lumped model, the coolant flows take into account the airfoil blade cooling, the cooling of the other hot components (disk cavities, shrouds, endwalls and platforms) and the action of the coolant as sealant flows (re-entering into the main stream); also the various temperatures of the heat transfer processes are calculated.